Electronic Supplementary Material (ESI) for Physical Chemistry Chemical Physics.

On the exploration of the melting behavior of metallic compounds and solid solutions via multiple classical molecular dynamics approaches: application to Al-based systems

Camille Rincent, Juan-Ricardo Castillo-Sánchez, Aïmen E. Gheribi, and Jean-Philippe Harvey*

**Corresponding Author:* jean-philippe.harvey@polymtl.ca

Centre for Research in Computational Thermochemistry (CRCT), Department of Chemical Engineering, Polytechnique Montréal, C.P. 6079, Succursale "Downtown", Montréal, Québec H3C 3A7, Canada.

1. IMPACT OF THE INITIAL LATTICE ON THE LATTICE EVOLUTION IN TIME

An energetic analysis of these defect-induced supercells was then performed to refine our critical assessment of these classical MD melting methods. Fig.S1 displays the relative increase in enthalpy of a supercell as a function of the concentration of vacancies for the random distribution method for Zn-HCP, Li-BCC and Cr-BCC. Each point on these curves was obtained after a NPT equilibration run at 300K for 0.11ns. Al-FCC and Li-BCC supercells both show an increase of their enthalpy as a function of the concentration of vacancies. Surprisingly, Zn-HCP presents an internal energy decrease upon the introduction of vacancies in its HCP lattice. This appears as a limitation of the interatomic potential proposed by Jang et al. [1]. It should be pointed out that Zn is a metal with very weak metallic bonds relatively to the other metals studied in the present work. Therefore, the MEAM formalism is not perfectly suited to describe this element when compared to the energetic description of transition metals which have stronger metallic bonds [2, 3]. A structural analysis of pure Zn simulations shows that the local structure around specific atoms changes from HCP to FCC upon the integration of vacancies in its perfect supercell which is accompanied by a decrease of the molar enthalpy of the system (figure S1). The important relative energetic contribution of the second nearest neighbors to the potential internal energy of the supercell evidenced in figure S2 is likely at the origin of this limitation. For Zn in the HCP structure, more than 25% of its cohesive energy is coming from second nearest neighbors.

The reference structure used to parameterize the interatomic potential also has a critical effect on these numerical melting simulations. The origin of this effect is shown in Fig.S3 for Zr which can be modelled with the interatomic potential proposed by Gheribi [4, 5] via a formulation with either an HCP or BCC reference structure. This figure shows that both interatomic potentials lead to an increase of the molar enthalpy when exploring the melting behavior of a BCC structure. For the HCP structure, the interatomic potential with the HCP reference structure behaves similarly to the one for Zn, i.e. an energetic stabilization of the supercell by local atomic rearrangements from HCP into FCC local ordering. A typical heating curve of Zr (modelled with an interatomic potential with a HCP reference structure) starting from a BCC supercell (upper panel) and HCP supercell (lower panel) with 1.0% and 0.5% of random vacancies respectively is presented in figure S4. This figure shows how a small concentration of vacancies allows the system to locally reorganize to favor its most energetically stable state. As an example, the original BCC lattice (BCC locally-ordered atoms coloured in blue) transforms into an HCP-dominated supercell (HCP locally-ordered atoms coloured in red). The MD simulation started with an HCP supercell (lower

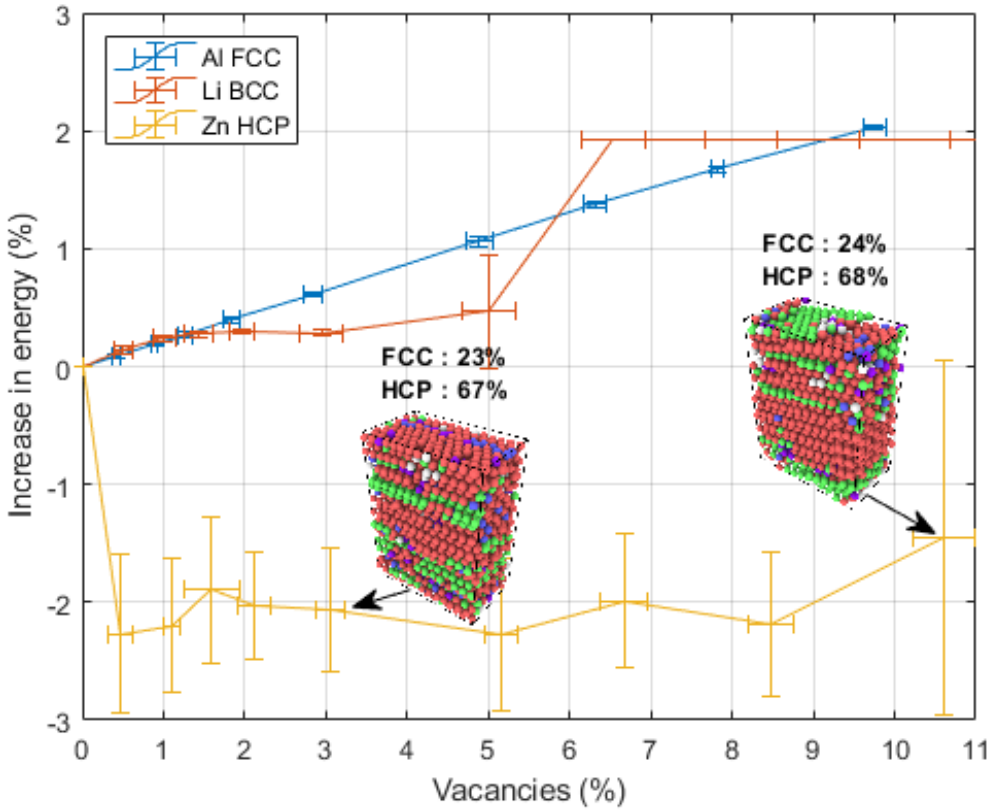

Fig. S1. Impact of the introduction of random vacancies on the energy of different lattice structures (i.e. Al-FCC, Li-BCC and Zn-HCP) after equilibrating the supercells at 400K for 0.11ns. Colors in the example supercell indicate each atom's short range ordering, red indicating HCP and green for FCC.

panel) kept its HCP local ordering up to melting. The methodology employed in the upper panel of Figure S4 reveals that the origin of the HCP-BCC allotropic transformation is connected to the metallurgical features of a polycrystalline material with vacancies. The α(HCP) $\rightarrow$ Zr-β(BCC) transformation occurs at 1135 K [6], which is consistent with the value observed in Figure S4 (blue line in the upper panel). Nevertheless, for melting purposes it appears that using the initial HCP configuration with no vacancies provides a better estimation of the melting point, which has been reported as 2128.15 K [7]. Note that the authors of the Zr-HCP potential reported a melting point of 1957 K using an interface velocity method [8], which is also lower than the experimental value reported in the literature.

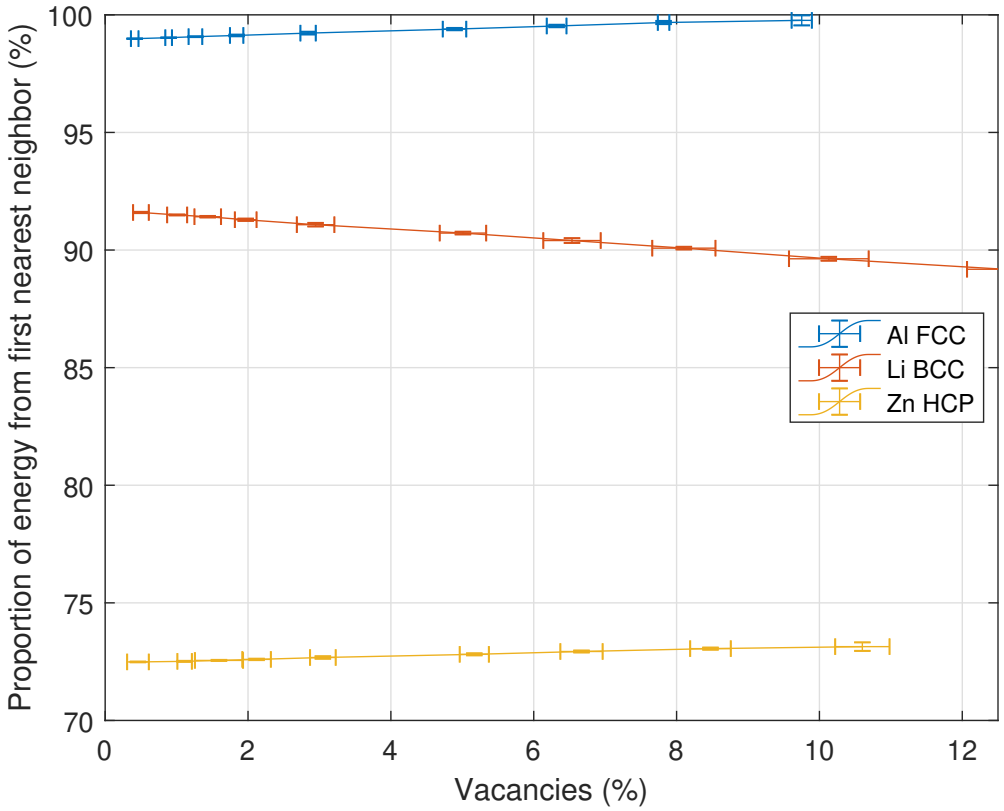

Fig. S2. Relative contribution to the internal energy generated of the first nearest neighbor when using the 2NN-MEAM formalism for Al, Li and Zn in their stable state after equilibrating at 300K for 0.11ns.

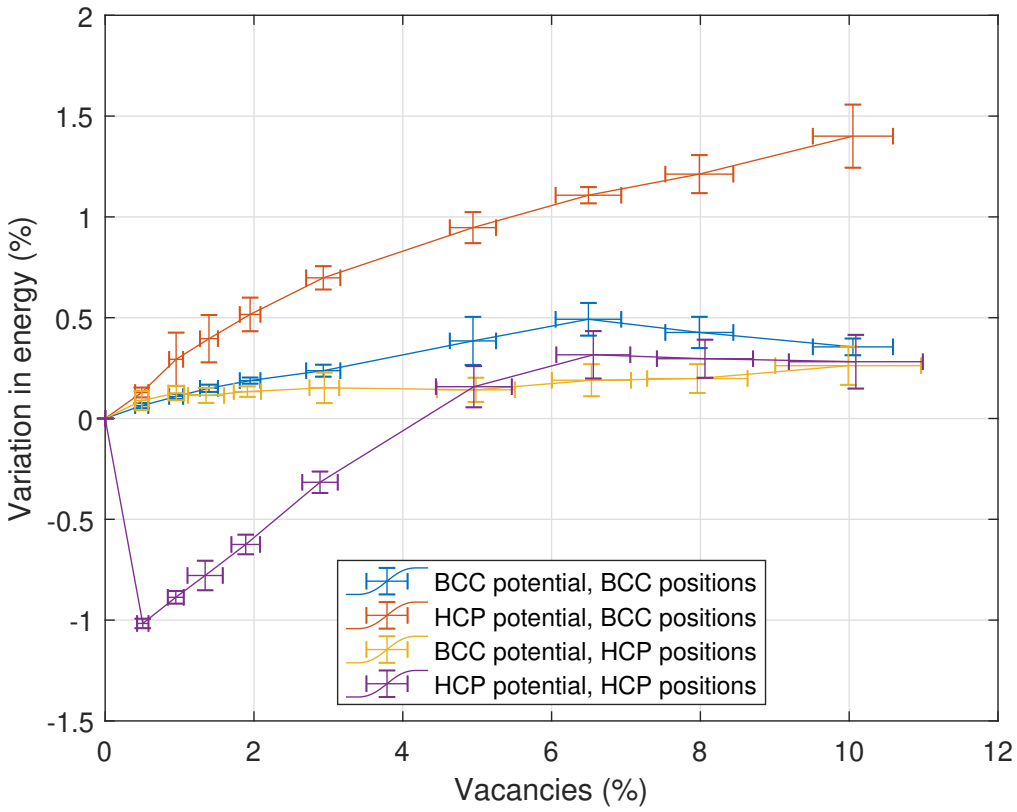

Fig. S3. Study on the impact of the difference in enthalpy against each respective reference structure after 0.11ns of equilibration at 400K between BCC-Zr and HCP-Zr structure in either the initial atomic positions of the lattice at its creation or as a reference structure for the inter-atomic potential used

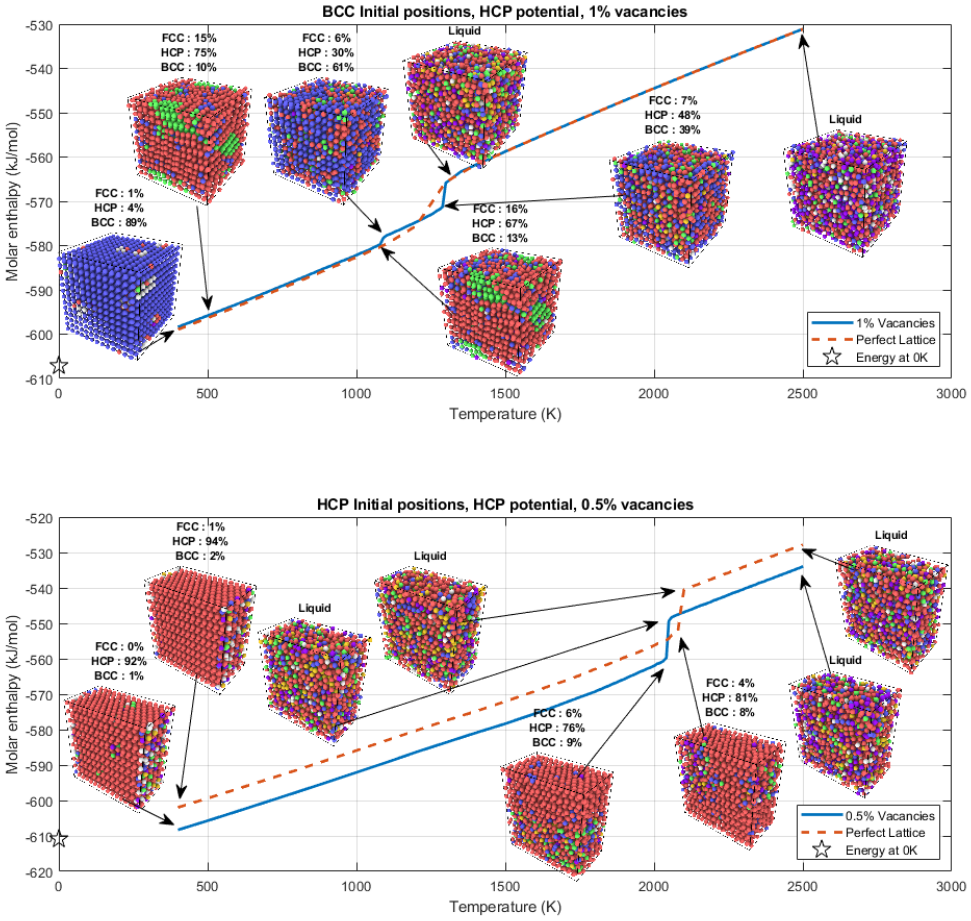

Fig. S4. Evolution of the molar enthalpy and of the local order as a function of temperature for both initial BCC and HCP structures using the Zr HCP-reference potential. Color represents local order, FCC is green, HCP is red, blue is BCC. First BCC-lattice with 1% random vacancies goes through two first order phase transition, the first one at 1085K and the second at 1285K. Second HCP-lattice with 0.5% random vacancies goes through a single phase transition at 2045K (opposed to 2090K for the perfect lattice) but the vacancies allows the lattice to minimize its energy and become more stable.

2. FORCE FIELD VALIDATION

In this section, we present the energetic predicting capabilities of the Al-Zr (derived from the Zr-BCC allotrope), Al-Li, and Al-Zn force fields developed in our main manuscript. Equilibrium Molecular Dynamic (EMD) simulations were performed for the solid and liquid aggregation states. EMD results were then compared to experimental data, critically assessed values, and first-principle calculations available in the literature.

A. Thermodynamic property evaluation

The molar enthalpy of mixing (Δh_{mix}) of liquid solutions was calculated using the following equation:

$$\Delta h_{mix}^{liq.} = h_{liq.} - \sum x_i h_i \tag{S1}$$

Where $h_{liq.}$ is the equilibrium enthalpy of the molten alloy, x_i and h_i are respectively the molar fraction and the molar enthalpy of the pure liquid of constituent "i" at the same temperature and pressure conditions.

The specific (molar) enthaply of formation at 0 K (Δh_f^{0K}) of solid phases was computed by the following equation:

$$\Delta h_f^{0K} = h_{comp}^{0K} - \sum x_i h_i^{SER-0K} \tag{S2}$$

Where h_{comp}^{0K} is the molar enthalpy of the compound, and x_i is the molar fraction of the "i" component within the solid phase. In all our calculations, the enthalpy of the solid structure at 0 K was obtained at a null pressure via a volume minimization of the studied supercell. Finally, h_i^{SER-0K} refers to the enthalpy of pure element i at 0 K under its Standard Element Reference state (SER-0K).

B. Enthalpy of mixing of binary liquid solutions

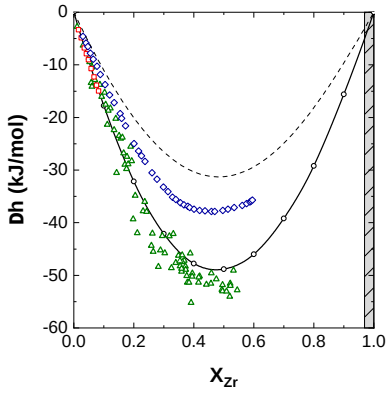

Fig. S5. Molar enthalpy of mixing for liquid Al-Zr using the BCC-allotrope as a reference structure for Zr-Zr interactions. Open circles and line are the thermodynamic data calculated with MD at T= 2000 K. Experimental data from Esin *et al.* [9] (diamonds) at 1970 K, Sudavtsova *et al.* [10] (squares) at 1790 K, and Witusiewicz *et al.* [11] (triangles) at 2080 K are presented as open symbols. The dashed line stands for the results at 2000 K from classical thermodynamics using FactSage [12]. The shaded grey zone corresponds to the meta-stability zone of the liquid at 2000K.

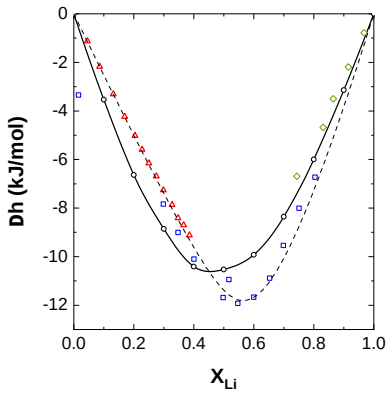

Fig. S6. Molar enthalpy of mixing for liquid Al-Li. Open circles and line stand for the thermodynamic data calculated with MD at T= 1000 K. Experimental data from Bushmaov *et al.* [13] (triangles) at 1023 K, Moser *et al.* [14] (squares) at 973 K, and Moser *et al.* [14] (diamonds) at 879 K are presented as open symbols. The dashed line stands for the results at 1000 K from classical thermodynamics using FactSage [12].

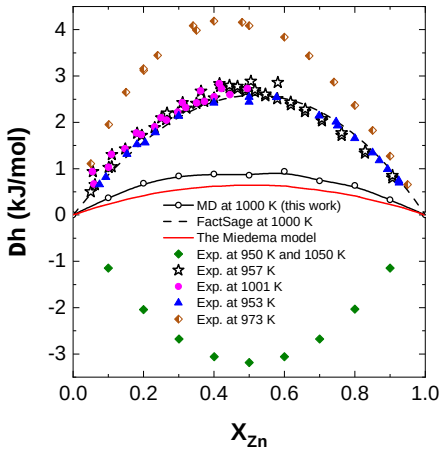

Fig. S7. Molar enthalpy of mixing for liquid Al-Zn. Black circles and line stand for the thermodynamic data calculated with MD at 1000 K. Experimental data from Lutz & Voigt [15] at 950 and 1050 K are shown as green diamonds. Data from Debski *et al.* [16] at 957 K and 1001 K are respectively presented by open stars and filled circles. Experimental measurements from Wittig & Keil at 953 K (triangles) and 973 K (semi-filled) are also displayed. The dashed line stands for the results at 1000 K from classical thermodynamics using FactSage [12]. The continuous black line represents the Miedema model [15, 17, 18].

C. Energetic description of solids

The enthalpy of formation for different Al-Zr, Al-Zn, and Al-Li compounds is presented in Table S1. Note that the Al-Zr interatomic potential was developed using the BCC allotrope to describe the Zr-Zr interactions. In this regard, the fourth column in Table S1 has been added to account for the HCP-BCC allotropic transformation. This is because the 0 K DFT data [19] considers the HCP structure as the Standard Element Reference (SER) for Zr.

Table S1. Enthapy of formation (Δh_f^{0K}) of different compounds from MD simulations compared with first-principle calculations. Formation energies are reported in eV/atom.

Formula	Space group	Δh_f^{0K} (this work)	Δh_f^{0K} - $x_{Zr}\, h_{\mathrm{hcp}\rightarrow\mathrm{bcc}}$ (this work)	DFT [19]
Zr_3Al	$Pm\bar{3}m$	-0.381	-0.325	-0.302
Zr_4Al_3	P6/mmm	-0.508	-0.465	-0.398
$ZrAl_3$	I4/mmm	-0.482	-0.463	-0.487
$ZrAl_3$	$Pm\bar{3}m$	-0.496	-0.477	-0.464
Al_2Zn	$P\bar{3}m1$	0.003	...	0.008
Al_3Zn	$Pm\bar{3}m$	0.000	...	0.025
Li_3Al	I4/mmm	-0.092	...	-0.080
Li_3Al_2	$R\bar{3}m$	-0.05	...	-0.187
Al_3Li	$Pm\bar{3}m$	-0124	...	-0.102

3. RADIAL DISTRIBUTION FUNCTION (RDF) OF PURE ALUMINIUM BEFORE AND AFTER MELTING

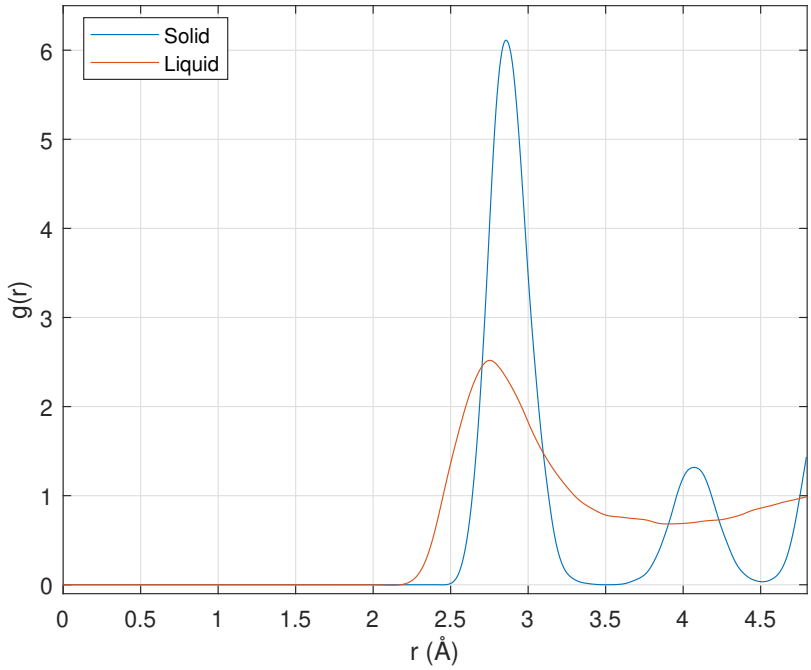

Fig. S8. Radial distribution function of pure aluminium at a solid state of 400K and after melting, at 1140K.

REFERENCES

1. H.-S. Jang, K.-M. Kim, and B.-J. Lee, "Modified embedded-atom method interatomic potentials for pure zn and mg-zn binary system," Calphad **60**, 200–207 (2018).
2. S. Ding and X. Wang, "A systematic study on the meam interatomic potentials of the transition metal nitrides tmns (tm=ti, v, cr, fe) binary systems," J. Alloy. Compd. **805**, 1081–1089 (2019).
3. B.-J. Lee, M. Baskes, H. Kim, and Y. Koo Cho, "Second nearest-neighbor modified embedded atom method potentials for bcc transition metals," Phys. Rev. B **64**, 184102 (2001).
4. A. E. Gheribi, "Molecular dynamics study of stable and undercooled liquid zirconium based on meam interatomic potential," Mater. Chem. Phys. **116**, 489–496 (2009).
5. J.-R. Castillo-Sánchez, A. Rincent, A. E. Gheribi, and J.-P. Harvey, "On the transferability of classical pairwise additive atomistic force field to the description of unary and multicomponent systems: applications to the solidification of al-based alloys," Phys. Chem. Chem. Phys. **24**, 22605–22623 (2022).
6. S. Banerjee, "Nuclear applications: Zirconium alloys," in *Encyclopedia of Materials: Science and Technology*, K. J. Buschow, R. W. Cahn, M. C. Flemings, B. Ilschner, E. J. Kramer, S. Mahajan, and P. Veyssière, eds. (Elsevier, Oxford, 2001), pp. 6287–6299.
7. D. Deardorff and E. T. Hayes, "Melting point determination of hafnium, zirconium, and titanium," JOM **8**, 509–510 (1956).
8. Y.-M. Kim, B.-J. Lee, and M. Baskes, "Modified embedded-atom method interatomic potentials for ti and zr," Phys. Rev. B **74**, 014101 (2006).
9. Y. O. Esin, N. Bobrov, M. Petrushevskij, and P. Gel'd, "Formation enthalpy of liquid aluminium alloys with titanium and zirconium," Izvestiya Akademii Nauk SSSR, Met. pp. 104–109 (1974).
10. V. Sudavtsova, G. Batalin, and V. Tutevich, "Thermodynamic properties of molten binary alloys in systems al–zr(nb, mo).(translation)," Russ. Met. pp. 183–185 (1985).
11. V. Witusiewicz, U. K. Stolz, I. Arpshofen, and F. Sommer, "Thermodynamics of liquid al-cu-zr alloys," Zeitschrift fuer Met. **89**, 704–713 (1998).
12. C. W. Bale, P. Chartrand, S. Degterov, G. Eriksson, K. Hack, R. B. Mahfoud, J. Melançon, A. Pelton, and S. Petersen, "Factsage thermochemical software and databases," Calphad **26**, 189–228 (2002).
13. V. Bushmanov and S. Yatsenko, "Thermodynamic properties of binary systems of lithium, sodium, potassium with aluminium, gallium, indium, thallium," Zhurnal Fizicheskoj Khimii **55**, 2951–2952 (1981).
14. Z. Moser, F. Sommer, and B. Predel, "Calorimetric studies of liquid al-li alloys/kalorimetrische untersuchung flüssiger al-li-legierungen," Int. J. Mater. Res. **79**, 705–707 (1988).
15. G. J. Lutz and A. F. Voigt, "A radioactive tracer dew point method for measuring vapor pressures of binary alloys. the zinc-aluminum system1," The J. Phys. Chem. **67**, 2795–2799 (1963).
16. A. Dębski, W. Gąsior, and K. Szmit, "Calorimetric measurements of liquid al-zn alloys," Metall. Mater. Transactions A **47**, 4933–4940 (2016).
17. F. R. De Boer, W. Mattens, R. Boom, A. Miedema, and A. Niessen, "Cohesion in metals. transition metal alloys," (1988).
18. A. Dębski, R. Dębski, and W. Gąsior, "New features of entall database: comparison of experimental and model formation enthalpies," Arch. Metall. Mater. **59** (2014).
19. A. Jain, S. P. Ong, G. Hautier, W. Chen, W. D. Richards, S. Dacek, S. Cholia, D. Gunter, D. Skinner, G. Ceder *et al.*, "Commentary: The materials project: A materials genome approach to accelerating materials innovation," APL materials **1**, 011002 (2013).